# Parallel adaptive procedure for CFD simulations

Imad Kissami<sup>1,\*</sup>, Souhail Maazioui<sup>1</sup>, Fayssal Benkhaldoun<sup>2</sup>

### **Abstract**

The present paper describes a parallel adaptive procedure in CFD solvers. The code dynamically refines and coarses the discretization for accurately resolution of the different features regarding the electron density. Our purpose is to examine the performance of A new parallel adaptive procedure introduced on the ADAPT platform, which resolve of a relatively complicated system coupling the flow partial differential equations to the Poisson's equation. The implementation deals with the MUMPS parallel multi-frontal direct solver and mesh partitioning methods using METIS to improve the performance of the framework. The standard MPI is used to establish communication between processors. Performance analysis of the parallel adaptive procedure shows the efficiency and the potential of the method for the transport equation coupled with Poisson's equation and for the propagation equations of ionization waves.

*Keywords:* Ionization waves, Finite volume methods, Adaptive mesh, MUMPS, METIS, Parallel computing

### 1. Introduction

Computational fluid dynamics, commonly known by the acronym 'CFD', has advanced rapidly over the last two decades and is today recognized as a valuable tool in all aspects of science, technology and industry. Nowadays, hundreds of software packages are used by engineers across a wide range of application and

<sup>\*</sup>Corresponding author

Email addresses: imad.kissami@um6p.ma (Imad Kissami),

souhail.maazioui@um6p.ma (Souhail Maazioui),

fayssal@math.univ-paris13.fr(Fayssal Benkhaldoun)

<sup>&</sup>lt;sup>1</sup>Mohammed VI Polytechnic University, Lot 990 Hay Moulay Rachid, Benguerir 43150, Morocco.

<sup>&</sup>lt;sup>2</sup>LAGA, Université Paris 13, 99 Av J.B. Clement, 93430 Villetaneuse, France.

research areas. The ultimate aim of CFD is to provide a description of fluids flows, at different levels of complexity, that must be at the same time economical and sufficiently complete. Recently, the availability of high-performance computing hardware had led to an upsurge of interest in more sophisticated mathematical models and increasingly complex and extensive computer simulations into the wider industrial community.

While experiments undertaken to investigate streamer propagation are costly and require sophisticated equipment, performing simulations often conduct an inquiry into the effect of a given process using relatively simple models. Mostly, numerical models of streamer discharges are formulated by coupling the electrostatic to the motion of charged particles (electrons, positive and negative ions) which lead to a system of equations coupling a set of convection—diffusion—reaction equations for charged particles to stationary Poisson's equation for the electric field. However, numerical computing for studying streamer propagation remains very expensive even with use of current vector supercomputers. Numerical simulation of ionization waves often presents difficulties due to their nonlinear form, presence of source terms, and coupling between the electron density and electric field. In addition, the difficulty in these models comes from the presence of both diffusion and convection terms which needs special discretization in some parts of the domain.

Distributed parallel computers have recently been successfully employed in large scale analysis for the numerical simulation of the streamer propagation in [7, 6], when the authors tackled the parallelization of 2D and 3D simulations of the streamer propagation in a static grid using the parallel solver MUMPS [1], METIS [5] for graph partitioning and the standard MPI to ensure the communications between processors. Kumar et al. [8] have also successfully studied similar problems to those presented in this paper. The associated linear systems have been solved using iterative Gmres and CG solvers [9]. One difference is that in our work we consider direct methods based on LU decomposition using the MUMPS solver.

In one of our earlier works, an adaptive analysis on unstructured discretization procedures was used in [2] to present an effective and accurate method in order to address this complex physical phenomenon. It was pointed out that considering unstructured mesh and suitable grid adaptation procedure makes the transition from 2D to 3D domains straightforward, especially when an object oriented programming approach is used. When applied to 2D model, this method proved to be efficient, whilst minor improvements are observed when the method is applied to 3D model, the latest still require heavy computational resources.

In this paper, we seek to show that mesh adaptation and parallelization methods can significantly speed up numerical calculations. The parallel adaptive procedure is applied for resolving the transport equation coupled with Poisson's equation in the general case, and particularly the propagation of an ionization wave in a rectangular domain subject to an electric field created by a difference in potentials between its walls. The obtained results demonstrate the efficiency of the proposed parallel adaptive finite volume method for this class of ionization wave front propagations. This work present investigations, results, and conclusions that will no doubt be useful to scientific community and engineers who are concerned with the various aspects of computational fluid mechanics.

The paper is organized as follows. In section 2, we introduce the aim some basic information about ADAPT platform and its positioning. In section 3, we discuss how the resulting discrete system, for the evolution equation coupled with Poisson's equation, can be effectively solved directly by combining adaptive mesh and parallel computing techniques in order to take advantage of those massively parallel clusters available to LAGA scientists. The implementation strategy of parrallelization is also explained in details. Section 4 includes numerical results and examples that prove the efficiency of our resolution method. Finally, concluding remarks are summarized in section 5.

### 2. The ADAPT framework

#### 2.1. Overview

The software name ADAPT [2, 7, 6] is an abbreviation of adaptation, which refers to the mesh adaptation strategy adopted in this object oriented platform along with the coupling between finite element and finite volume methods. As a CFD (Computational Fluid Dynamics) software, this framework has been developed for realizing numerical simulations on an unstructured and adaptative mesh for large scale CFD applications.

The existing ADAPT implementation is a parallel C++ code for each phenomenon using fixed grid. The code requires very fine mesh to perform a 3D simulation. Running a 3D streamer code, for instance, may take more than 8 hours while using 512 cores. Given this purpose, we decided to mix the automatic adaptive procedure to the parallelization. This paper is an important step towards this direction, it represents 2D results of streamer equations using parallel adaptive procedure.

### 2.2. Working environment

To realize all the experiments, both sequential and parallel, we worked on the MAGI cluster http://www.univ-paris13.fr/calcul/wiki which is located at the University of Paris 13 (Villetaneuse, France). This machine contains about 50 Dell FC430 blades with 10 Hyper-Threading dual processor cores (40 cores per blade), and 64 GB RAM per blade interconnected by InfiniBand.

## 3. Parallel approach

### 3.1. Governing equations

As a starting point, we consider the evolution equation coupled with the Poisson equation, written as:

$$\begin{cases} \frac{\partial u}{\partial t} + F(V, u) = S, \\ \Delta P = b. \end{cases}$$
 (1)

given that  $F(V, u) = div(u.\overrightarrow{V}) - \Delta u$ , S = 0, and  $V = \overrightarrow{\nabla} P$ , the previous system yields:

$$\begin{cases} \frac{\partial u}{\partial t} + div(u.\overrightarrow{V}) = \Delta u \\ \Delta P = b. \end{cases}$$
 (2)

The first equation is discretized using the finite volume method on an unstructured triangular mesh. The time-integration of the transport equation is performed using an explicit scheme. The discretized form of Poisson's equation leads to a linear algebraic system. We obtain the following set of equations:

$$\begin{cases}
u_i^{n+1} = u_i^n - \frac{\Delta t}{\mu_i} \underbrace{\sum_{j=1}^m u_{ij} \overrightarrow{V}_{ij} \overrightarrow{n}_{ij} |\sigma_{ij}|}_{Rez\_conv} + \underbrace{\frac{\Delta t}{\mu_i} \sum_{j=1}^m \overrightarrow{\nabla} u_{ij} \overrightarrow{n}_{ij} |\sigma_{ij}|}_{Rez\_dissip} \\
\mathbf{A} \cdot \overrightarrow{P}^n = \overrightarrow{b}^n
\end{cases}$$
(3)

where m is the number of faces of volume  $\mu_i$ ,  $\overrightarrow{n}_{ij}$  is the unit normal vector on the face  $\sigma_{ij}$  (face between volumes  $\mu_i$  and  $\mu_j$ ) and  $|\sigma_{ij}|$  is the face's lenght. Other variables denoted by subscript ij represent variables on the face  $\sigma_{ij}$ . **A** is a large sparse matrix which contains coefficients that depend only on the grid topology.

### 3.2. Domain decomposition and linear system A.P = b solver

The 2D adaptive unstructured mesh in Figure 1 was decomposed into four sub-domains using the **METIS** algorithm. These partitions have approximately the same size, which is a good property since the workload is balanced on the homogeneous processors of our platform. To solve the linear system, the parallel solver **MUMPS** is used. The current approach with **MUMPS** shows significant advantages by avoiding problems related to pre-conditioners, and requiring fewer iterations to converge to the solution.

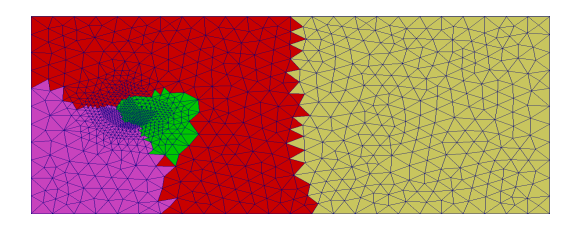


Figure 1: Decomposition of the adaptive discretization into 4 sub-domains using the METIS algorithm.

#### 3.3. Parallel discretization of the evolution equation

### 3.3.1. Parallel computation of $u_{ij}$ on face $\sigma_{ij}$

The convective flux  $u_{ij}$  in the equation 3 is computed using simple upwind scheme

$$u_{ij} = \begin{cases} u_i & if(\overrightarrow{u_{ij}} \cdot \overrightarrow{n_{ij}}) \ge 0 \\ u_j & in \ other \ case, \end{cases}$$
 (4)

Here, we assume that the normal vector  $\overrightarrow{n_{ij}}$  is oriented from the cell  $T_i$  to the cell  $T_j$ . The computation of the drift velocity  $\overrightarrow{u_{ij}}$  on the face  $\sigma_{ij}$  will be explained further ahead, in algorithm 1.

# **Algorithm 1:** Compute $u_{ij}$ on face $\sigma_{ij}$

```
1 F:number of faces;
2 for k := 1 to F do
       if dot(V_k.n_k) >= 0 then
           u_k = \tilde{u_i};
4
       end
5
       else
6
7
           if \sigma k is inner faces then
                u_k = \tilde{u_i};
8
           end
9
10
            else if \sigma k is halo faces then
                u_k = 	ilde{u_h}; /\star \ 	ilde{u_h}: halo value sent by neighbor
11
                 subdomain
           end
12
       end
13
14 end
```

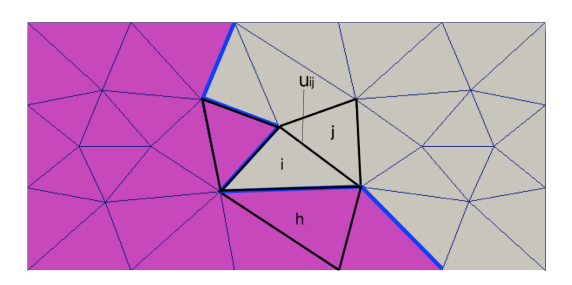


Figure 2: Computation of  $u_{ij}$  in mesh splitted into two subdomains

### Higher order approximation in space

The upwind scheme has a first order of accuracy. It leads to a high numerical dissipation that needs to be reduced using a higher order algorithm. The scheme is therefore extended by a Van Leer's type MUSCL algorithm along with Barth-Jespersen limiter.

One introduces  $\tilde{u_i}$ ,  $\tilde{u_j}$  in the equation 4 instead of  $u_i$ ,  $u_j$ 

$$\widetilde{u}_i = u_i + \psi_i.(\overrightarrow{\nabla}u_i.\overrightarrow{r_i})$$

$$\widetilde{u}_j = u_j + \psi_j.(\overrightarrow{\nabla}u_j.\overrightarrow{r_j})$$

In figure 2, we considered the case where the mesh is splitted into two subdomains, then we computed  $u_{ij}$  on the face  $\sigma_{ij}$ . For a given face  $\sigma_k$ , it is supposed that  $T_i$  and  $T_j$  are, respectively, the cells on the left and the right of  $\sigma_k$ . Let's note  $\sigma_k = \sigma_{ij}$  and  $u_k = u_{ij}$ . The algorithm 1 shows how the  $u_{ij}$  is computed on face  $\sigma_{ij}$ .

where  $\overrightarrow{\nabla} u_i$ ,  $\overrightarrow{\nabla} u_j$  are gradients of u on cells  $T_i$ ,  $T_j$ . We can compute the gradients assuming that u is a piecewise linear function and its value  $u_i$  is in the center of gravity of the cell  $T_i$ . This linear function is computed by the least square method which include all neighboring cells of  $T_i$  (neighbors with at least one common vertex).  $\overrightarrow{r_i}$  is a vector oriented from the center of gravity of the cell  $T_i$  to the center of gravity of a face  $\sigma_{ij}$ . similarly,  $\overrightarrow{r_j}$  is a vector oriented from the center of gravity of the cell  $T_j$  to the center of gravity of the face  $\sigma_{ij}$ .  $\psi_i$  and  $\psi_j$  are Barth-Jespersen limiter function [3]. One can compute the gradient  $\overrightarrow{\nabla} u_i < (u_i)_x, (u_i)_y >$  (for cell  $T_i$ ) as follow

$$(u_i)_x = \frac{I_{yy}.J_x - I_{xy}.Jy}{D}, \quad (u_i)_y = \frac{I_{xx}.J_y - I_{xy}.Jx}{D}$$
 (5)

where

$$I_{xx} = \sum_{j=1}^{n} (x_j - x_i)^2, \quad I_{yy} = \sum_{j=1}^{n} (y_j - y_i)^2,$$

$$I_{xy} = \sum_{j=1}^{n} (x_j - x_i)(y_j - y_i), \quad J_x = \sum_{j=1}^{n} (u_j - u_i)(x_j - x_i),$$

$$J_y = \sum_{j=1}^{n} (u_j - u_i)(y_j - y_i), \quad D = I_{xx}.I_{yy} - I_{xy}^2$$
(6)

where  $u_i(u_j)$  is the value of u on cell  $T_i(T_j)$  and n is the number of neighbor cells with at least one common vertex.

Figure 3 represents all neighbor cells needed to compute the gradient of u. The inner information are represented by  $u_i$  (j={1,...,6}) and halo cells by  $u_h$ 

 $(h=\{1,...,8\}).$ 

### **Algorithm 2:** Compute the gradient $(u)_x$ on cell

```
1 C: number of cells;
2 I_{xx}, I_{yy},D: computed using mesh;
3 A_x = sqrt(I_{xx}), A_y = sqrt(I_{yy});
 4 for i:=1 to C do
         for j:=1 to inner cells neighbor by node do
              J_x = J_x + (A_x * (u[j] - u[i]));
              J_{v} = J_{v} + (A_{v} * (u[j] - u[i]));
 7
 8
         for h:=1 to halo cells neighbor by node do
              J_x = J_x + (A_x * (u[h] - u[i]));
10
              J_{y} = J_{y} + (A_{y} * (u[h] - u[i]));
11
12
         (u)_{x}[i] = \frac{(A_{x}^{2}*J_{x} - A_{x}*A_{y}*J_{y})}{D}

(u)_{y}[i] = \frac{(A_{y}^{2}*J_{y} - A_{x}*A_{y}*J_{x})}{D}
13
15 end
```

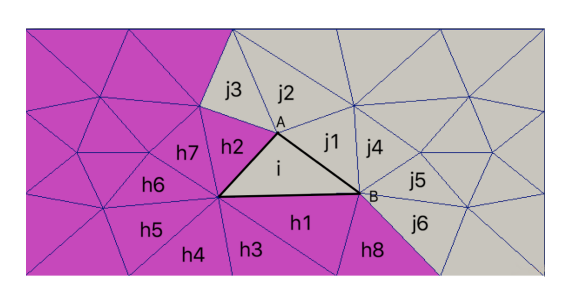


Figure 3: Computation of  $\nabla u_i$  in mesh splitted into two subdomains

## 3.3.2. Parallel computation of the gradient $\nabla u_{ij}$ on face $\sigma_{ij}$

The gradient  $\overrightarrow{\nabla} u_{ij}$  is computed using the diamond cell appearing in Figure 4 constructed by connection of centers of gravity (i, j) of cells  $T_i$ ,  $T_j$  which share the face  $\sigma_{ij}$  and its endpoints A, B, the gradient can be written as follow

$$\overrightarrow{\nabla}u_{ij} = \frac{1}{2\mu(D_{\sigma_{ij}})}[(u_A - u_B)\overrightarrow{n}_{LR}|\sigma_{LR}| + (u_j - u_i)\overrightarrow{n}_{ij}|\sigma_{ij}|]$$
(7)

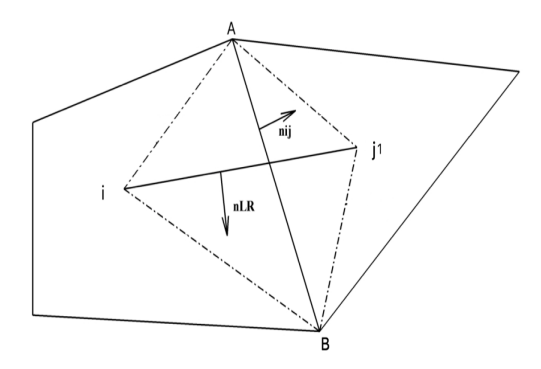


Figure 4: Illustration of control volumes and Diamond cell used in the space discretization.

The values of  $u_A$ ,  $u_B$  on the face  $\sigma_{ij}$  end points are computed using the least square method. The algorithm 2 shows how it is done.

$$u_A = \sum_{p=1}^{N(A)} = \alpha_p(A)u_p, \quad u_B = \sum_{p=1}^{N(B)} = \alpha_p(B)u_p$$
 (8)

where  $u_p$  is the value of the solution u in the cell  $T_p$ , N(A) and N(B) are ,respectively, the number of cells including vertex A and B,  $\alpha_p(A)$  and  $\alpha_p(B)$  are the weights obtained using the least square method. One can write for vertex A:

$$\alpha_i(A) = \frac{1 + \lambda_x(x_i - x_A) + \lambda_y(y_i - y_A)}{N(A) + \lambda_x R_x + \lambda_y R_y}$$
(9)

with

$$I_{xx} = \sum_{p=1}^{N(A)} (x_p - x_A)^2, \quad I_{yy} = \sum_{p=1}^{N(A)} (y_j - y_A)^2,$$

$$I_{xy} = \sum_{p=1}^{N(A)} (x_p - x_A)(y_p - y_A), \quad J_x = \sum_{p=1}^{N(A)} (u_p - u_A)(x_p - x_A),$$

$$R_x = \sum_{p=1}^{N(A)} (x_p - x_A), \quad R_x = \sum_{p=1}^{N(A)} (y_p - y_A),$$

$$\lambda_x = \frac{I_{xy}R_y + I_{yy}R_x}{D}, \lambda_y = \frac{I_{xy}R_x + I_{xx}R_y}{D}.$$
(10)

## **Algorithm 3:** Compute value on node A $(u_A)$

```
1 u_A:double;
2 N :number of nodes;
3 Alpha: weight coming from the least square method;
4 for n := 1 to N do
      for c:=1 to inner cells around node n do
5
          u_A(n) += Alpha(c) * u_i(c);
 6
7
      end
      for m:=1 to halo cells around node do
8
          u_A(n) += Alpha(m) * u_h(m);
 9
      end
10
11 end
12 return u_{node};
```

# **Algorithm 4:** Compute $\nabla u_{ij}$ on face ij

```
1 F:number of faces;
    \overrightarrow{\nabla} u: Vector 2d:
 3 for k := 1 to F do
           A:first node of face;
           B:second face node;
 5
           i:center of gravity of cell T_i;
 6
          j:center of gravity of cell T_j;
 7
          mes = \frac{1}{2\mu(D_{\sigma_{ii}})};
 8
          if Inner faces then
 9
                 \overrightarrow{\nabla} u(k) = mes * (u_A - u_B) \overrightarrow{n}_{LR} |\sigma_{LR}| + (u_j - u_i) \overrightarrow{n}_{ij} |\sigma_{ij}|;
10
           end
11
           else if Halo faces then
12
                 \overrightarrow{\nabla} u(k) = mes * (u_A - u_B) \overrightarrow{n}_{LR} |\sigma_{LR}| + (u_h - u_i) \overrightarrow{n}_{ih} |\sigma_{ih}|;
13
           end
14
15 end
16 return \overrightarrow{\nabla} u;
```

### 3.4. Parallel adaptive procedure

To improve the performance of the finite volume method, we incorporate a dynamic mesh adaptation using the gradient of the solution *u*. Algorithm 5 summarizes the parallelization procedure using mesh refinement. It provides a piece of pseudocode that shows how the parallelization of adaptive code is done according to the coupling of evolution equation with Poisson's equation.

We can observe that most parts of the code are parallel (line 24, line 9 to 11 and line 27 to 31) except reading and splitting mesh procedure at the beginning and between lines 16 and 20. Indeed, at this step, we compute the adaptation criterion which depends on the gradient of the solution u, we refine mesh, and we construct matrix A (1) that will be used to solve the linear system in line 24. Matrix A is computed at each adaptation step because it depends only on the mesh.

Our contribution will serve to enhance the performance of 3D simulations, in which we consider the same type of equations and strategy. It is worth noting that the structure of the 3D grid will be more complex because tetrahedra are used instead of triangles. Using the adaptive 3D version may take up to 3 weeks to give results.

```
Algorithm 5: Algorithm of parallel ADAPT
```

```
1 W:double;
2 if rank==0 then /* for the master processor
      Read mesh data;
3
      Split mesh with METIS;
      Distribute mesh to all processors;
6 end
7 W=0;
8 for each rank do /★ for each processor
                                                            */
      Initialize conditions and create constants;
      Send the informations of halos cells to neighbor
10
       subdomains;
      Apply boundary conditions;
11
12 end
13 for each iteration do
      if Solution evolved enough then
         if rank = = 0 then
15
             Compute Adaptation Criteria;
16
             Adapt the mesh: Refine where necessary and
17
               coarsen where necessary;
             Split and distribute mesh to all processors;
18
             Construct matrix of linear system;
19
             Split the matrix and send part of each processor;
20
         end
21
22
      end
      for all rank do /∗ for all processors
                                                            */
23
          Solve linear system using MUMPS;
24
      end
25
      for each rank do
26
          Send the informations of halos cells to neighbor
27
           subdomains;
          Apply boundary conditions;
28
          Compute fluxes of convection, diffusion and source
29
           term;
          Update solution : W^{n+1} =
30
           W^n + \Delta t * (rez\_conv + rez\_dissip + rez\_source);
          Save results in parallel way using Paraview;
31
      end
32
                         12
33 end
```

### 4. Numerical examples

### 4.1. Transport equation

The first example consists of a simple transport equation coupled with poisson equation in two dimensions.

$$\frac{\partial u}{\partial t} + \operatorname{div}(u\vec{v}) = 0, 
-\operatorname{div}(\nabla P) = 0, 
\vec{v} = -\vec{\nabla} P,$$
(11)

To assess the parallel performance of the proposed parallel adaptive procedure, we solve the test example of transport equation in (11). The initial condition is represented by Gaussian pulse with maximum magnitude of 1.

$$u(x,y,0) = \exp\left(-\frac{(x-0.2)^2 + (y-0.25)^2}{0.02^2}\right),$$

### **Boundary conditions**

$$\frac{\partial u}{\partial \vec{n}} = 0 \qquad for \ x = 0, \ x = 1,$$

$$V = 1[V] \qquad for \ x = 0,$$

$$V = 0[V] \qquad for \ x = 1.$$

In Figure 5, we present the numerical results obtained using the parallel adaptive procedure with 32 MPI cores, solution u at two different times. It is easy to constat that the parallel adaptive procedure for the finite volume method resolved this test example and accurately captured the physical features. The criteria for mesh adaptation is based only on the gradient of the solution u.

To further illustrate these effects, we display Figure 6 with cross-sections. The results on the very fine mesh are assumed as reference solutions and relative errors are calculated and summarized in Table 1. For the considered test example, the parallel adaptive finite volume method is highly accurate and efficient, compare the errors and computational times in Table 1.

Table 2 summarizes the comparison between the parallel version of transport equation using fixed mesh and the parallel one using adaptive mesh. We can observe that using 32 MPI cores the parallel adaptive code takes less than 447

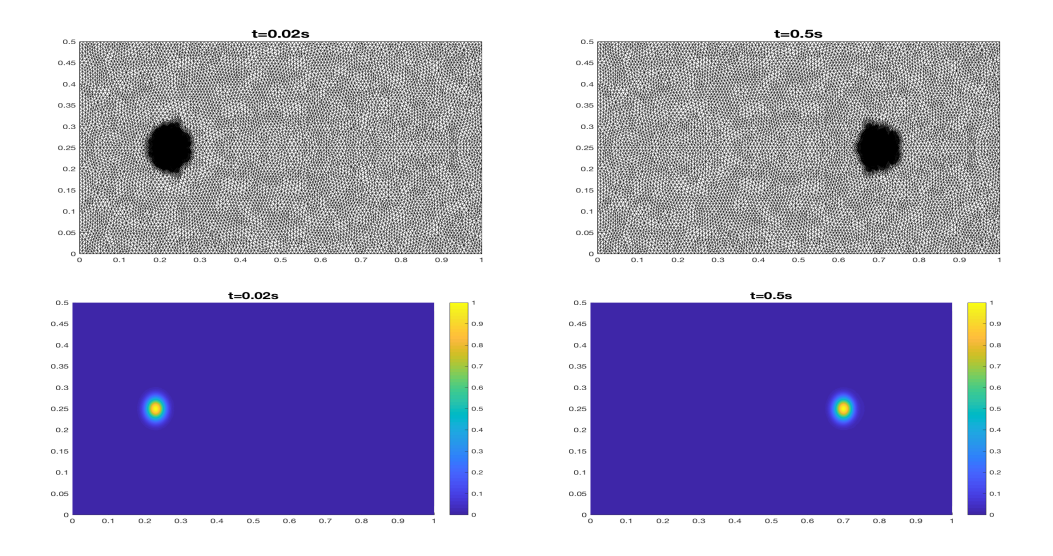


Figure 5: Adaptive meshes (first row), solution u distributions (second row) in the rectangular domain at times t = 0.02 and 0.5 s.

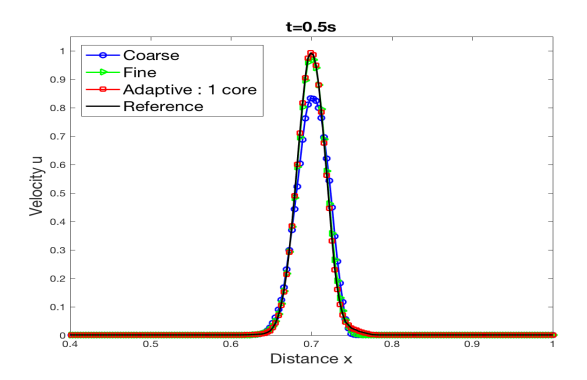


Figure 6: Cross-section at x = 0.25 cm of the solution u at time 0.5 s.

secondes ( $\sim$  8 minutes) minutes instead of 6264 seconds ( $\sim$  1 hour 44 minutes) using parallel code with fixed mesh and 256 MPI cores.

|           | # of cores | # of cells | # of nodes | Error in <i>u</i> | CPU time |
|-----------|------------|------------|------------|-------------------|----------|
| Coarse    | 1          | 43674      | 22061      | 0.1573            | 2619     |
| Fine      | 1          | 297600     | 149505     | 0.0310            | 22570    |
| Adaptive  | 1          | 44862      | 22784      | 0.0009            | 6263     |
| Reference | 1          | 1190400    | 596609     |                   | 230130   |

Table 1: Mesh statistics, relative errors and computational times (in seconds) for propagation of a discharge in the rectangular domain at time t = 0.5 s.

| # of cores | CPU time (in seconds) |            |  |
|------------|-----------------------|------------|--|
|            | Adaptive mesh         | Fixed mesh |  |
| 1          | 6263                  | 230130     |  |
| 2          | 3441                  | 121121     |  |
| 4          | 1842                  | 63 925     |  |
| 8          | 1138                  | 32875      |  |
| 16         | 782                   | 16676      |  |
| 32         | 447                   | 8851       |  |
| 64         | -                     | 4602       |  |
| 128        | -                     | 2557       |  |
| 256        | -                     | 1424       |  |

Table 2: Computational times for the transport equation coupled with poisson equation using parallel adaptive procedure

### 4.2. Equations for streamer propagation

Here, we are interested in a simple two-dimensional model for negative streamer investigated in [2] among others. Since the charged particles can be considered as continuum, the particles are dealt with in form of densities and we can use continuum mechanics for them. Hence as mentioned above, this model is able to capture the streamer propagation and consists of a convection-diffusion-reaction equation for the electron density along coupled with the Poisson's equation for the electric potential. In what follows, we use boldface notation to denote vectors. Hence, for the electron density  $n_e$ , the ion density  $n_i$ , the electric potential V and the electric

field  $\vec{E}$ , we solve the following equations

$$\frac{\partial n_e}{\partial t} + \operatorname{div}\left(n_e \vec{v}_e - D_e \vec{\nabla} n_e\right) = S_e, 
\frac{\partial n_i}{\partial t} = S_i^+, 
-\operatorname{div}(\varepsilon \nabla V) = e(n_i - n_e), 
\vec{E} = -\vec{\nabla} V,$$
(12)

where  $\vec{v}_e$  the electron drift velocity,  $D_e$  the diffusive coefficient,  $\varepsilon$  the dielectric constant, e the electron charge,  $S_e$  and  $S_i^+$  are source terms. The electron drift velocity  $\vec{v}_e$  is a function of the electric field  $\vec{E}$  and depends on the ratio  $||\vec{E}||/N$ , with N is the neutral gas density

$$\vec{v}_e = -\left(C_1 \frac{\|\vec{E}\|}{N} + C_2\right) \frac{\vec{E}}{\|\vec{E}\|}.$$
 (13)

The diffusion coefficient  $D_e$  is a function of the electron drift velocity and the electric field

$$D_e = \left(0.3341 \times 10^9 \left(\frac{\|\vec{E}\|}{N}\right)^{0.54069}\right) \frac{\|\vec{v}_e\|}{\|\vec{E}\|}.$$
 (14)

The source terms in (13) depend on the electron drift velocity and the electron density

$$S_e = S_i^+ = \alpha ||\vec{v}_e|| n_e N,$$
 (15)

where the coefficient  $\alpha$  is defined by the following formula

$$\alpha = C_3 \exp\left(\frac{C_4}{\|\vec{E}\|/N}\right). \tag{16}$$

The constants  $C_1$ ,  $C_2$ ,  $C_3$  and  $C_4$  appeared in above equations are defined by empirical formulae in [2]. Note that the equations (13)-(16) has to be solved in a time interval and a two-dimensional bounded spatial domain equipped with given boundary and initial conditions.

Here, we solve the test example of discharge propagation in a homogeneous electric field described in [2]. Hence, we solve equations (12) in the rectangular domain  $[0,1] \times [0,0.5]$  subjected to a plane anode with  $V = 25000 \ volts$  on the

left and a plane cathode with V = 0 volts on the right whereas periodic boundary conditions are imposed on the upper and lower walls. Initially,

$$n_e(x, y, 0) = n_i(x, y, 0) = 10^{16} \times e^{-\frac{(x - 0.2)^2 + (y - 0.25)^2}{\sigma^2}} + 10^9,$$

with  $\sigma = 0.01$ . All our simulations are carried on the MAGI cluster. For the mesh adaptation we used our technique used for combustion simulations in [4].

Figure 7 depicts the numerical results obtained using the parallel adaptive procedure with 32 MPI cores, distribution of electron densities  $n_e$  and the velocity fields  $\vec{v}_e$  at two different times. The parallel adaptive procedure for the finite volume method resolved this case successfully and accurately captured the physical features similarly to the first example. Here, the criteria for mesh adaptation is based on the gradient of the ion density  $n_e$  and the source term  $S_e$ .

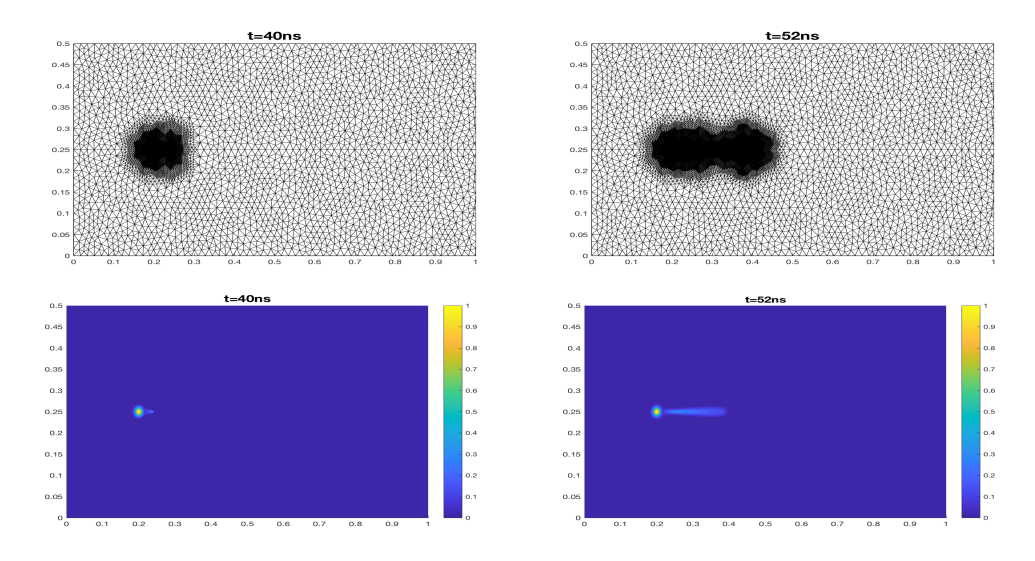


Figure 7: Adaptive meshes (first row), electron density distributions (second row) for propagation of a discharge in the rectangular domain at times t = 40 and 52 ns.

To underline these effects, we illustrate the mesh adaptation in Figure 8. The results on the very fine mesh are assumed as reference solutions and relative errors are calculated and summarized in Table 3. For the considered test example, the parallel adaptive finite volume method is highly accurate and efficient. Resulting errors and computational times are compared in Table 3.

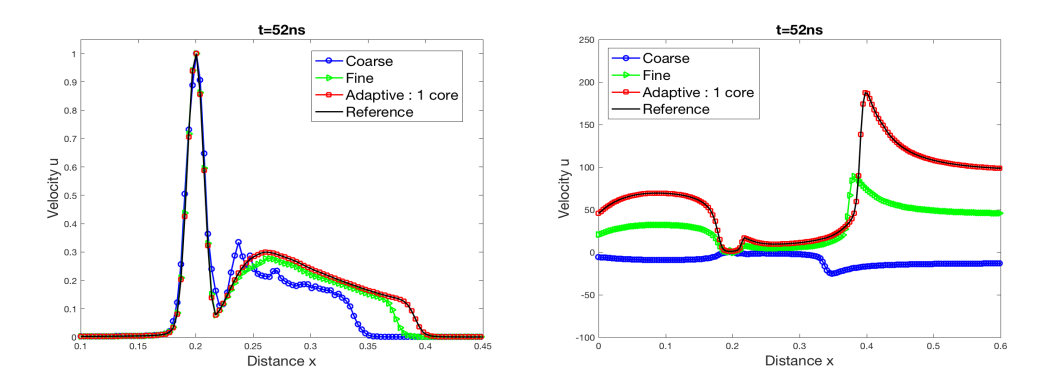


Figure 8: Cross-section at x = 0.25 cm of the electron density (left) and velocity (right) at time 52 ns.

|           | # of cores | # of cells | # of nodes | Error in $n_e$ | Error in $\vec{v}_e$ | CPU time |
|-----------|------------|------------|------------|----------------|----------------------|----------|
| Coarse    | 1          | 43674      | 22061      | 0.3104         | 1.4747               | 6860     |
| Fine      | 1          | 297600     | 149505     | 0.0924         | 0.4387               | 31315    |
| Adaptive  | 1          | 46156      | 23167      | 0.0013         | 0.0041               | 18340    |
| Reference | 1          | 1190400    | 596609     |                |                      | 291600   |

Table 3: Mesh statistics, relative errors and computational times (in seconds) for propagation of a discharge in the rectangular domain at time t = 52 ns.

In table 4, a comparison is made between the parallel version of 2D streamer using fixed mesh and the parallel one using adaptive mesh. We can observe that using 32 MPI cores, the parallel adaptive code take 1147 ( $\sim$ 19 minutes) instead of 18340 ( $\sim$  5 hours) using parallel code with fixed mesh and 256 MPI cores.

| # of cores | CPU time (in seconds) |            |  |
|------------|-----------------------|------------|--|
|            | Adaptive mesh         | Fixed mesh |  |
| 1          | 18340                 | 291600     |  |
| 2          | 9968                  | 153473     |  |
| 4          | 5394                  | 81000      |  |
| 8          | 3056                  | 41657      |  |
| 16         | 1834                  | 21130      |  |
| 32         | 1147                  | 11215      |  |
| 64         | -                     | 5832       |  |
| 128        | -                     | 3240       |  |
| 256        | -                     | 1944       |  |

Table 4: Computational times for propagation of a discharge using parallel adaptive procedure

#### 5. Conclusion

We have proposed a new parallel adaptive procedure for finite volume solution of ionization waves in planar electric fields. Numerical results have been presented for the transport equation coupled with Poisson equation and a for the propagation of ionization waves in a rectangular domain. The originality of this work lies in the runnning of parallel code using dynamic mesh adaptation. The workflow is realized: (1) using external tools such as METIS for mesh partitioning in order to enable the computational load balance for the global assembly, (2) using MPI to assure communication, (3) using MUMPS solver to solve the system of linear equations. (4) using adaptive procedure to avoid the use of very fine mesh. In summary, the most important advantage of the presented schemes is the potential to produce highly accurate solutions at low computational cost.

We conclude that the campaign of numerical tests yields expected results, meaning that our parallel implementation goes into the right direction at the moment and thus contributes significantly to employment of such methods. Overall, this approach seems to be a suitable tool for solving complex multidimensional streamer problems which require a huge calculation time. These findings can be exploited to achieve accurate 3D simulation of the streamer discharge with a reasonable computation cost, which allow for more realistic real-life geometries analysis. This part is the subject of an ongoing investigation that is to be published in our future works.

#### References

- [1] Amestoy, P., Duff, I.S., L'Excellent, J., Koster, J.: MUMPS: A general purpose distributed memory sparse solver. In: Applied Parallel Computing, New Paradigms for HPC in Industry and Academia, 5th International Workshop, PARA 2000 Bergen, Norway, June 18-20, 2000 Proceedings, pp. 121–130 (2000)
- [2] Benkhaldoun, F., Fořt, J., Hassouni, K., Karel, J.: Simulation of planar ionization wave front propagation on an unstructured adaptive grid. J. Comput. Appl. Math. **236**, 4623–4634 (2012)
- [3] Blazek, J.: Computational fluid dynamics: principles and applications. Butterworth-Heinemann (2015)
- [4] Elmahi, I., Benkhaldoun, F., Borghi, R., Raghay, S.: Ignition of fuel issuing from a porous cylinder located adjacent to a heated wall: a numerical study. Combust. Theory Modelling **8**, 789–809 (2004)
- [5] Karypis, G., Kumar, V.: A fast and high quality multilevel scheme for partitioning irregular graphs. SIAM J. Sci. Comput. 20(1), 359–392 (1998). DOI 10.1137/S1064827595287997. URL http://dx.doi.org/10.1137/S1064827595287997
- [6] Kissami, I., Cérin, C., Benkhaldoun, F., Scarella, G.: Parallelization of the ADAPT 3d streamer propagation code. In: 2016 IEEE Intl Conference on Computational Science and Engineering, CSE 2016, and IEEE Intl Conference on Embedded and Ubiquitous Computing, EUC 2016, and 15th Intl Symposium on Distributed Computing and Applications for Business Engineering, DCABES 2016, Paris, France, August 24-26, 2016, pp. 242–245. IEEE Computer Society (2016). DOI 10.1109/CSE-EUC-DCABES.2016. 191. URL https://doi.org/10.1109/CSE-EUC-DCABES.2016. 191
- [7] Kissami, I., Cérin, C., Benkhaldoun, F., Scarella, G.: Towards parallel CFD computation for the ADAPT framework. In: J. Carretero, J.G. Blas, R.K.L. Ko, P. Mueller, K. Nakano (eds.) Algorithms and Architectures for Parallel Processing 16th International Conference, ICA3PP 2016, Granada, Spain, December 14-16, 2016, Proceedings, *Lecture Notes in Computer Science*, vol. 10048, pp. 374–387. Springer (2016). DOI 10.1007/978-3-319-49583-5\\_28. URL https://doi.org/10.1007/978-3-319-49583-5\_28

- [8] Kumar, P., Markidis, S., Lapenta, G., Meerbergen, K., Roose, D.: High performance solvers for implicit particle in cell simulation. Procedia Computer Science 18, 2251–2258 (2013)
- [9] Saad, Y., Schultz, M.H.: Gmres: A generalized minimal residual algorithm for solving nonsymmetric linear systems. SIAM Journal on Scientific and Statistical Computing 7(3), 856–869 (1986). DOI 10.1137/0907058. URL http://dx.doi.org/10.1137/0907058